Surface reflectivity from the Ozone Monitoring Instrument using the Moderate Resolution Imaging Spectroradiometer to eliminate clouds: Effects of snow on ultraviolet and visible trace gas retrievals

G. O'Byrne,[1] R. V. Martin,[1,2] A. van Donkelaar,[1] J. Joiner,[3] and E. A. Celarier[4]

Received 24 August 2009; revised 5 February 2010; accepted 12 April 2010; published 8 September 2010.

[1] Satellite retrievals of tropospheric composition from measurements of solar backscatter require accurate information about surface reflectivity. We use clear-sky data from the Ozone Monitoring Instrument (OMI) to determine global surface reflectivity under both snow-covered and snow-free conditions at 354 nm. Clear-sky scenes are determined using cloud and aerosol data from the Moderate Resolution Imaging Spectroradiometer/Aqua satellite instrument that flies 12 min ahead of OMI/Aura. The result is a database of OMI-observed Lambertian equivalent reflectivity (LER) that does not rely on statistical methods to eliminate cloud and aerosol contamination. We apply this database to evaluate previous climatologies of surface reflectivity. Except for regions of seasonal snow cover, agreement is best with a climatology from OMI, which selects the surface reflectivity from a histogram of observed LER (mean difference, 0.0002; standard deviation, 0.011). Three other climatologies of surface reflectivity from Total Ozone Mapping Spectrometer, Global Ozone Monitoring Experiment, and OMI, based on minimum observed LER, are less consistent with our cloud- and aerosol-filtered data set (mean difference, −0.008, 0.012, and −0.002; standard deviation, 0.022, 0.026, and 0.033). Snow increases the sensitivity of solar backscatter measurements at ultraviolet and visible wavelengths to trace gases in the lower troposphere. However, all four existing LER climatologies poorly represent seasonal snow. Surface reflectivity over snow-covered lands depends strongly on the vegetation type covering the surface. The monthly variation of snow-covered reflectivity varies by less than 0.1 in fall and winter. Applying our snow-covered surface reflectivity database to OMI NO_2 retrievals could change the retrieved NO_2 column by 20%–50% over large regions with seasonal snow cover.

Citation: O'Byrne, G., R. V. Martin, A. van Donkelaar, J. Joiner, and E. A. Celarier (2010), Surface reflectivity from the Ozone Monitoring Instrument using the Moderate Resolution Imaging Spectroradiometer to eliminate clouds: Effects of snow on ultraviolet and visible trace gas retrievals, *J. Geophys. Res.*, *115*, D17305, doi:10.1029/2009JD013079.

1. Introduction

[2] Satellite observations provide global information about atmospheric constituents that is valuable to improve our understanding of climate and air quality. Measurements of solar backscattered radiation at ultraviolet and visible (UV-Vis) wavelengths from instruments such as Total Ozone Mapping Spectrometer (TOMS), Global Ozone Monitoring Experiment (GOME), GOME-2, Scanning Imaging Absorption Spectrometer for Atmospheric Cartography (SCIAMACHY), and Ozone Monitoring Instrument (OMI) have been applied to retrieve many important atmospheric constituents including O_3, NO_2, HCHO, SO_2, BrO, clouds, and aerosols [*Wagner et al.*, 2008]. These UV-Vis satellite observations provide valuable insight into the tropospheric composition of remote regions [*Krueger*, 1983; *Fishman et al.*, 1991; *Herman et al.*, 1997; *Chance*, 1998; *Richter and Burrows*, 2002], into trace gas emissions [*Beirle et al.*, 2003; *Martin et al.*, 2003; *Palmer et al.*, 2003; *Müller and Stavrakou*, 2005; *Richter et al.*, 2005; *Boersma et al.*, 2008], and into surface air quality [*Fishman et al.*, 2008; *Lamsal et al.*, 2008; *Martin*, 2008]. However, accurate description of the surface reflectivity is needed for retrievals of trace gases, clouds, and aerosol in the UV-Vis.

[3] The retrieval of trace gas abundances commonly begins with a spectral fit that is applied to distinctive absorption bands in the measured reflectance spectra [*Stutz and Platt*, 1996; *Chance*, 2006]. The observed absorption is used to calculate the slant column (SC), a measure of the

[1]Department of Physics and Atmospheric Science, Dalhousie University, Halifax, Nova Scotia, Canada.
[2]Also at Harvard-Smithsonian Center for Astrophysics, Cambridge, Massachusetts, USA.
[3]NASA Goddard Space Flight Center, Greenbelt, Maryland, USA.
[4]Goddard Earth Sciences and Technology Center, University of Maryland Baltimore County, Baltimore, Maryland, USA.

0148-0227/10/2009JD013079

total amount of trace gas along the path of the backscattered sunlight captured by the satellite instrument. A slant column is converted into a vertical column (VC), the integrated column above the surface, through use of an air mass factor (AMF) such that VC = SC/AMF [*Palmer et al.*, 2001]. The AMF accounts for the varying vertical sensitivity of the measurement, which depends on the light path through the atmosphere, the surface reflectivity, the trace gas vertical profile, clouds, and aerosols. In practice, the AMF is estimated using imperfect knowledge of these parameters and radiative transfer in the atmosphere.

[4] Previous studies have found a high sensitivity of the retrieval to surface reflectivity. *Lee et al.* [2009] estimate an error of 10%–20% in their SO_2 columns for an error of 0.02 in the surface reflectivity over land. For this same error in the surface reflectivity, *Boersma et al.* [2004] estimate an error of 15% in the derived tropospheric NO_2 column for polluted scenes. For a typical scene, *Koelemeijer et al.* [2001] estimate an error of 0.02 in the cloud fraction due to an error of 0.02 in the surface reflectivity. The reflectivity of snow is an important parameter in satellite-based estimation of surface UV irradiance [*Krotkov et al.*, 2001].

[5] Several global climatologies of surface reflectivity have been created from long-term data sets of measured radiances from TOMS [*Herman and Celarier*, 1997], GOME [*Koelemeijer et al.*, 2003], and OMI [*Kleipool et al.*, 2008]. Statistics are applied to the long-term data set to remove the effects of clouds and aerosols from measured reflectivity. This statistical cloud screening could lead to ambiguity in the absolute surface reflectivity. The NASA A-Train is a formation of several specialized satellites flying in close proximity which includes the instruments OMI and Moderate Resolution Imaging Spectroradiometer (MODIS). The wealth of information provided by these instruments over the same locations at nearly the same time grants an unprecedented opportunity to infer surface reflectivity, without statistical methods to eliminate clouds, and to evaluate the above data sets.

[6] Clouds and the surface often are modeled as opaque Lambertian reflectors for the purpose of satellite retrievals [*Acarreta et al.*, 2004]. In this approach, the wavelength specific, normalized backscattered radiance at the top of the atmosphere I_{TOA} is given by [*Davé*, 1964, equation 6.16; *Joiner and Vasilkov*, 2006]

$$I_{\mathrm{TOA}} = I_{\mathrm{TOA}}(R=0) + \frac{RI_g\gamma}{(1-RS_b)}, \tag{1}$$

where R is the Lambertian equivalent reflectivity (LER) of the cloud or surface, I_{g} is the total irradiance reaching the surface, γ is the transmittance of the atmosphere to reflected radiance, and S_{b} is the fraction of the reflected irradiance (or flux) that the atmosphere scatters back toward the reflector. The independent pixel approximation is used to deal with partially cloudy scenes. In this approximation, the total observed radiance (I_{Total}) is the sum of the top of atmosphere (TOA) radiances of the clear (I_{clear}) and cloudy (I_{cloud}) subpixels weighted by a cloud fraction (f). The total observed radiance is then expressed as

$$I_{\mathrm{Total}} = I_{\mathrm{Cloud}}\, f + I_{\mathrm{Clear}}(1-f). \tag{2}$$

For UV-Vis trace gas retrievals, the cloud fraction is determined by comparing the observed TOA radiance to the modeled clear-sky TOA radiance based on the climatological surface reflectivity. A deficit in the modeled TOA radiance is accounted for by clouds (which are typically more reflective than the surface). In practice, a small, highly reflective cloud and a large, semitransparent cloud with the same total reflectivity are indistinguishable. For this reason, the reflectivity of the modeled cloud is fixed and only the cloud fraction is allowed to vary. The cloud fraction (or effective cloud fraction) is thus a combination of the true geometrical cloud fraction and the cloud reflectivity. Typical choices for the cloud reflectivity are 0.6 and 0.8, which correspond to optically thick (highly reflective) clouds. An optimal Lambertian cloud model will approximate the transmission and reflection of a real cloud [*Stammes et al.*, 2008]. Snow cover poses a significant challenge for solar backscatter measurements of trace gases, as it can greatly change the radiative properties of the surface on short time scales (hours). The lack of contrast between snow and cloud in the UV-Vis also makes it difficult to infer cloud cover.

[7] In this work, we use cloud- and aerosol-filtered observations from OMI to determine global surface reflectivity under both snow-covered and snow-free conditions. Section 2 provides a brief description of the satellite instruments and data sets used in our analysis. Section 3 describes our cloud and aerosol screening techniques and applies them to retrieve the global surface reflectivity. Section 4 assesses the surface reflectivity over snow-covered lands. Section 5 investigates the implications of our snow-covered surface reflectivity on UV-Vis trace gas retrievals using NO_2 as an example.

2. Instruments and Data

[8] The Ozone Monitoring Instrument (OMI) is a Dutch/Finnish imaging spectrograph that measures the solar and Earth radiance spectrum from 270 to 500 nm [*Levelt et al.*, 2006]. OMI has a ground pixel resolution of 13 km × 24 km at nadir and a 114° swath, which allows for daily global coverage. OMI is on board the NASA Aura satellite that launched in July 2004. Aura is part of the A-Train constellation of satellites in polar orbits with equator crossing times near 1330 local time.

[9] NO_2 is retrieved from OMI measurements over 405–465 nm where NO_2 absorbs strongly, and there is little interference from other trace gases. Two OMI NO_2 products exist, the standard product [*Bucsela et al.*, 2006] and the DOMINO product [*Boersma et al.*, 2007]. There are also two OMI cloud products [*Acarreta et al.*, 2004; *Joiner and Vasilkov*, 2006]. Both NO_2 retrievals use a cloud product based on absorption from the O_2-O_2 collision complex (OMCLDO2) [*Acarreta et al.*, 2004; *Sneep et al.*, 2008]. The currently available Collection 3 products originally used surface LERs taken from the climatology of *Koelemeijer et al.* [2001], based on 5.5 years of GOME measurements. Use of the *Kleipool et al.* [2008] LER climatology has been implemented as of orbit number 24349 (11 February 2009) in both NO_2 products and is planned for future versions of the NO_2 products.

[10] The OMI cloud and NO_2 retrievals use the near real-time ice concentration and snow extent (NISE) data set (*Nolin et al.* [1998], updated daily) to infer snow coverage.

The NISE data set uses microwave measurements from the Special Sensor Microwave/Imager (SSM/I) instrument on board the DMSP F13 satellite. Because of its near-polar, Sun-synchronous orbit, the frequency of observations by the SSM/I is greater than 1/d above 55°. The principle of the snow detection algorithm is based on the scattering of microwave radiation, emitted from the underlying soil, by snow grains [*Armstrong and Brodzik*, 2001, 2002; *Chang et al.*, 2002]. Wet snow emits microwave radiation similar to the underlying surface and so is not detected in this way. The NISE data set has not been validated but is known to consistently miss thin snow cover. A snow flag is provided in the OMI product, which indicates if a scene contains dry snow according to the NISE data set. For many scenes flagged as dry snow by the NISE data set, the current OMI cloud and NO_2 retrievals replace the climatological surface LER with a value of 0.6 to account for increased reflectivity due to snow.

[11] The Moderate Resolution Imaging Spectroradiometer (MODIS) is an instrument currently on board two NASA satellites, Terra and Aqua. MODIS measures radiances in 36 spectral bands from 0.415 to 14.235 μm at high spatial resolution [*Salomonson et al.*, 1989]. The nadir spatial resolution varies between bands from 250 to 1 km. Each MODIS instrument takes measurements over the entire globe every 1–2 days. Aqua was launched in May 2002 into a near-polar, Sun-synchronous orbit with a 1330 local overpass time. It was the first member of the A-Train.

[12] In this study, we use three MODIS Collection 5 Level-2 data products: the cloud mask [*Ackerman et al.*, 1998], the cloud optical depth [*Platnick et al.*, 2003], and the aerosol optical depth (AOD) [*Remer et al.*, 2005]. The AOD product uses the first seven spectral bands (0.47–2.13 μm), while the cloud products use additional bands at infrared wavelengths. Recent validation studies indicate that the MODIS cloud mask performs well except over polar regions at night [*Berendes et al.*, 2004; *Ackerman et al.*, 2008]. The MODIS cloud mask follows a separate set of tests when the possibility of snow is detected. These snow-covered scenes are of particular interest to the current study. In their comparison with an arctic ground-based lidar and radar, *Liu et al.* [2004] report that during the day MODIS/Terra misidentifies 2.7% of cloudy scenes as clear sky and 6.9% clear-sky scenes as cloudy.

3. Climatology of Cloud- and Aerosol-Filtered Snow-Free Surface LER

3.1. Development of the Climatology

[13] The retrieval of surface reflectivity from OMI measurements requires accurate assessment of the fraction of TOA radiance that was reflected by atmospheric constituents versus the fraction from the surface. In particular, information is needed about clouds and aerosols, which are spatially inhomogeneous and significantly reflective. Because the OMI cloud and aerosol products depend on the a priori surface reflectivity, additional information is required to retrieve the surface reflectivity. In this study, the MODIS cloud and aerosol masks are used to determine the presence of clouds and aerosols within the OMI field of view. Using MODIS to screen the atmospheric constituents permits detection of clear-sky OMI scenes without the use of statistical methods to eliminate cloud and aerosol contamination, even when surface LER is unknown.

[14] We regrid the MODIS cloud mask onto a 0.25° × 0.25° grid for each orbit. All grid cells containing measurements flagged as cloudy or uncertain in the MODIS cloud mask are designated as cloudy. We account for horizontal displacement of the clouds during the time between the MODIS and OMI overpass ($t_{\text{MODIS-OMI}} \sim 15$ min) by flagging all grid squares, to which a cloud could have propagated, as potentially cloudy. We use the maximum tropospheric wind vectors ($v_{\max}$) at the cloud location from the NASA Goddard Earth Observing System GEOS 5 assimilated meteorological data. For each cloudy grid cell, all grid cells up to a distance $v_{\max} \times t_{\text{MODIS-OMI}}$ away in each direction are also flagged as contaminated. We similarly use the MODIS AOD product to screen for aerosol. All 0.25° grid points containing a pixel with an AOD greater than 0.2 are flagged as contaminated and allowed to propagate to a distance $v_{\max} \times t_{\text{MODIS-OMI}}$. Lowering the tolerance for AOD to 0.05 yields no noticeable difference in the remaining results.

[15] We apply the cloud/aerosol mask to check each OMI pixel in the same orbit for possible contamination. OMI pixels that do not intersect a flagged cell are considered clear-sky scenes. OMI pixels that extend beyond the MODIS swath are rejected. We use this database of cloud- and aerosol-filtered OMI scenes to create a climatology of surface reflectivity. For clear-sky scenes, the retrieval of the surface LER becomes a simple inversion of equation (1), where $I_{\text{TOA}}(R = 0)$ is equal to the Rayleigh scattering of the atmosphere.

[16] We use the scene LERs provided in the OMI Rotational Raman (OMCLDRR) cloud product [*Joiner and Vasilkov*, 2006] at 354 nm (346–354 nm) as measurements of surface LER for cloud- and aerosol-filtered scenes. When the OMCLDRR cloud fraction is less than 5%, the LER model is used (as opposed to the mixed LER approach) and an effective scene pressure is retrieved. This is the case for the majority of our cloud-free scenes; however, greater cloud fractions remain due to incorrect characterization of the surface reflectivity in the cloud retrieval. We eliminate scenes with retrieved pressures that differ by more than 100 hPa from the surface pressure to further exclude residual aerosols and clouds that prevent light from traveling through the full extent of the atmosphere (removes 23% of remaining measurements). We exclude data that are flagged as potentially affected by Sun glint (removes 24% of remaining measurements) and use the NISE data set to eliminate snow cover. Finally, we exclude outliers with scene LERs greater than 0.3 to eliminate residual snow cover and remaining occurrences of direct reflection. This last criterion removes 0.14% of the remaining measurements.

[17] Figure 1 shows the mean measured surface reflectivity using 3 years of data (2005, 2006, and 2007) at 0.5° × 0.5° resolution. Ocean surface LERs are typically in the range of 0.05–0.10. The reflectivity of oceans is largely governed by suspended particles and phytoplankton since water itself absorbs weakly at UV wavelengths [*Herman and Celarier*, 1997; *Koelemeijer et al.*, 2003]. Over land the surface LER is typically in the range of 0.01–0.10. Absorption by chlorophyll leads to vegetated regions being darker, whereas deserts are brighter (LERs up to 0.2). Shadowing in moun-

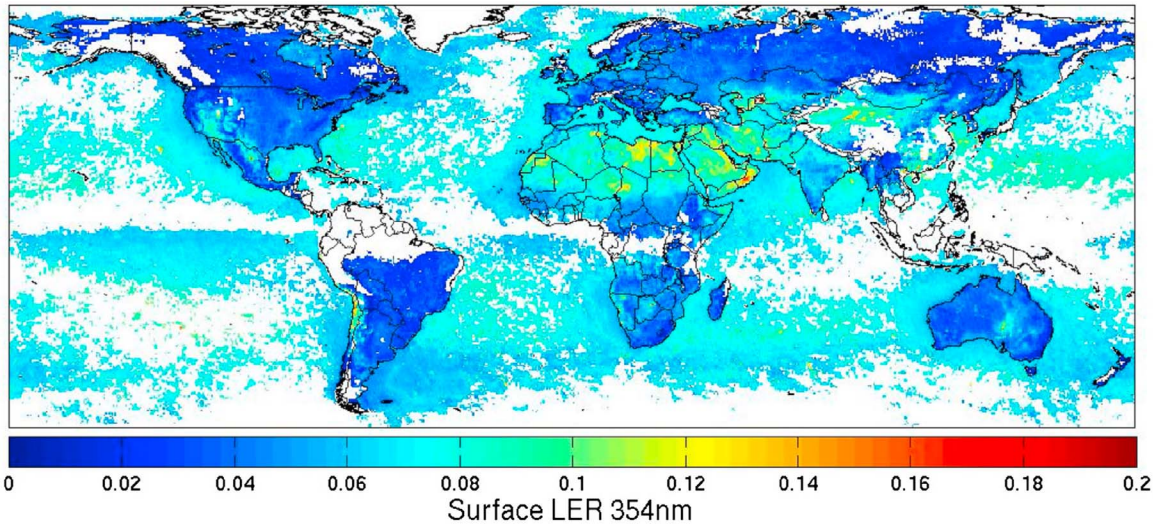

Figure 1. OMI-derived surface Lambertian equivalent reflectivity (LER) at 354 nm from a 3 year (2005–2007) database of clear-sky scenes. Clear-sky scenes are determined by cloud and aerosol observations from the MODIS instrument on board the Aqua satellite, which measures the same scenes within 12 min of OMI. White locations on the map are areas where less than 10 suitable measurements were available over the 3 year period.

tainous regions causes the LER to reach values near zero. White areas indicate where persistent cloud or aerosol lead to little or no data after filtering. Between 60°N and 60°S, 20% of the grid cells in Figure 1 contain less than 10 valid measurements.

[18] We estimate the precision on the values in Figure 1 by examining the variability of the measured LERs in each grid cell. Over land, the standard error of the mean is typically 0.005. This estimate includes contributions from the subpixel variation in surface LER and variation in the bidirectional reflectance function. Over oceans, where there are fewer measurements, the standard error increases to 0.01. Radiometric uncertainty additionally contributes to the total error.

3.2. Comparison With Existing Climatologies

[19] We use our cloud- and aerosol-filtered surface LER data set to evaluate three previous climatologies used in satellite retrievals of atmospheric constituents. *Herman and Celarier* [1997] derive surface LERs at 1° × 1.25° resolution based on minimum observed radiances in the 340–380 nm window from 14.5 years of TOMS data (henceforth referred to as TOMS MinLER). *Koelemeijer et al.* [2003] derive surface LERs at 1° × 1° resolution based on minimum observed radiances from GOME over a 5.5 year period (henceforth referred to as GOME MinLER). We interpolate between the GOME MinLER values at 335 and 380 nm to estimate the LERs at 354 nm before comparing to our cloud- and aerosol-filtered reflectivities. *Kleipool et al.* [2008] produce two climatologies of surface reflectivity at 0.5° × 0.5° resolution from 3 years of OMI radiances. The first climatology is also based on minimum observed radiances (henceforth referred to as OMI MinLER). They argue, however, that the minimum surface LER may not be the most appropriate value since the minimum could occur due to darkening by precipitation or shading from cloud or ground. Also, the minimum is likely to select the lowest value in the bidirectional reflectance distribution function (BRDF). For their second climatology (henceforth referred to as OMI LER), a histogram of measured scene LERs is created for each grid point around the globe. The surface LER is typically chosen as either the mode or the 1% cumulative probable value of the histogram. The OMI LER product allows for more than minimal seasonal snow cover. We ignore regions where this is permitted in our evaluation with our strictly snow-free climatology.

[20] We calculate the surface LERs from our cloud-free data set at the resolution of each of the four climatologies. We calculate monthly differences between our product and these previous climatologies and then average to produce seasonal and annual differences.

[21] Table 1 summarizes the comparison. All four of the annual global mean climatologies are within 0.01 of our cloud- and aerosol-filtered product. Our product is more consistent with the OMI LER product than the OMI MinLER product. This supports the selection of surface LERs using a histogram rather than choosing the minimum. However, when scenes with more than minimal seasonal snow cover are included, the OMI LER is less consistent with our data set (mean difference, 0.01; standard deviation, 0.07). The GOME MinLER climatology is higher on average by 0.01 than our cloud- and aerosol-filtered product. A possible explanation is residual cloud in the GOME climatology that arises from the large pixel size and the relatively few measurements used in constructing the climatology. The 14.5 year data set used in the construction of the TOMS MinLER yields lower surface LERs than our cloud- and aerosol-filtered product. Differences in radiometric calibration could contribute to interinstrument differences. The difference in local overpass times between OMI (1345), TOMS (~1200), and GOME (1030) is unlikely to explain the observed discrepancies since the OMI-TOMS difference is opposite in sign from the OMI-GOME difference.

Table 1. Comparison of Four Previous Climatologies Minus Our Cloud- and Aerosol-Filtered Data Set Which Uses OMI Reflectivity Data at 354 nm[a]

Previous Climatology	OMI LER (unitless)	OMI MinLER (unitless)	GOME MinLER (unitless)	TOMS MinLER (unitless)
Mean difference	0.0002	−0.006	0.009	−0.011
Standard deviation	0.011	0.033	0.026	0.022
Mean difference over land	0.003	−0.007	0.009	−0.009
Mean difference over ocean	−0.002	−0.005	0.009	−0.012
Mean difference (DJF)	−0.0003	−0.005	0.009	−0.010
Mean difference (MAM)	−0.002	−0.007	0.009	−0.013
Mean difference (JJA)	0.001	−0.004	0.009	−0.013
Mean difference (SON)	−0.0003	−0.006	0.009	−0.009

[a]Monthly differences are calculated and then averaged to produce annual and seasonal differences. OMI LER and OMI MinLER were compiled by *Kleipool et al.* [2008] using OMI data (1330 overpass) at 354 nm for 2005–2007. GOME MinLER was produced by *Koelemeijer et al.* [2003] using GOME data (1030 overpass) for 1995–2000. We perform a linear interpolation between 335 and 380 nm to produce a GOME MinLER data set at 354 nm. TOMS MinLER was compiled by *Herman and Celarier* [1997] using TOMS/Nimbus 7 data (period 104.15 min, near noon overpass) between 340 and 380 nm for the years 1979–1993.

[22] Figure 2 shows the mean seasonal differences in surface LER between our product and three of the previous climatologies; OMI MinLER is omitted. Differences with the OMI LER climatology for remote oceans are typically within 0.01, while coastal OMI LER values tend to be lower by up to 0.03. Vegetated regions over land are generally higher in the OMI LER product by 0.01–0.02. In regions where higher dust loading is expected [*Miller et al.*, 2006], the OMI LER is generally lower by 0.01–0.03. Suspended dust lowers the apparent reflectivity [*Herman et al.*, 1997; *Torres et al.*, 1998] and could contribute to the difference. Although we screen for aerosols using MODIS AOD and by neglecting measurements with high scene pressures, persistent thin aerosol layers could still affect our product. This implies the difference between OMI LER and the true LER could be even larger. The GOME and TOMS MinLER climatologies are distinctly lower in areas of enhanced dust aerosol. In particular, TOMS MinLER is lower by more then

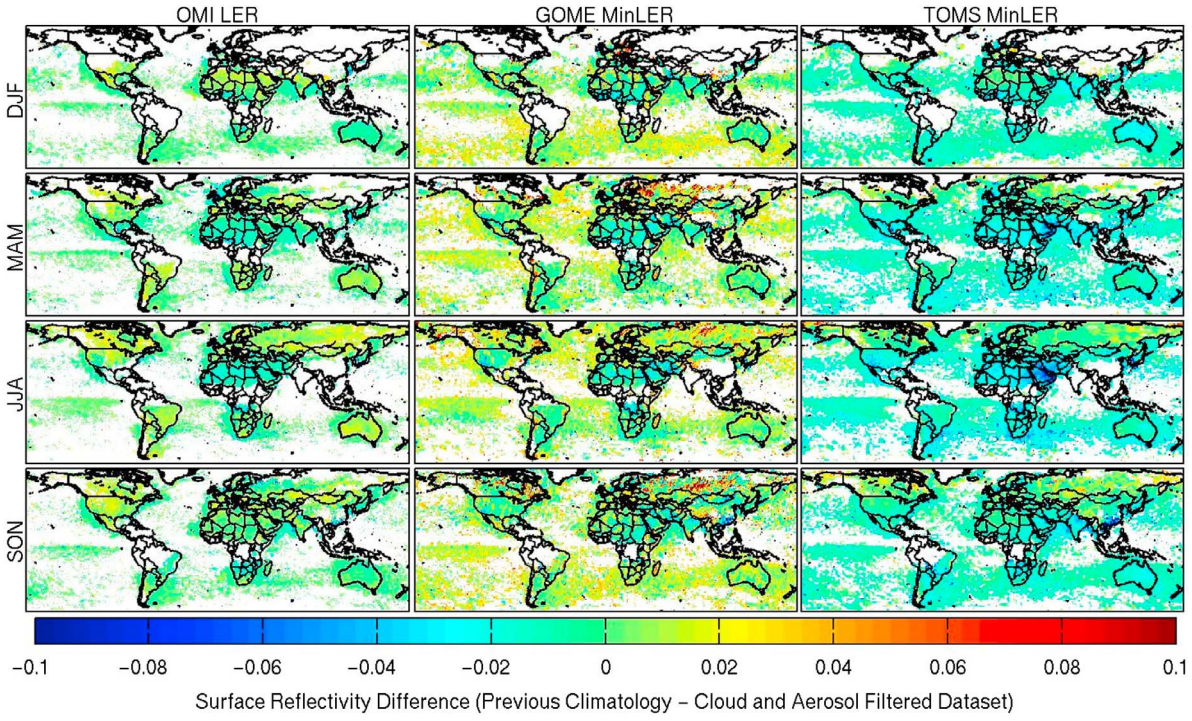

Figure 2. Seasonal mean comparison of our cloud- and aerosol-filtered surface LER data set (354 nm) to three previous climatologies of surface LER. (left) A comparison to the climatology of *Kleipool et al.* [2008] at 0.5° × 0.5° resolution based on 3 years of OMI measurements (354 nm). (middle) A comparison to the climatology of *Koelemeijer et al.* [2003] at 1° × 1° resolution based on 5 years of GOME measurements (interpolated 354 nm). (right) A comparison to the climatology of *Herman and Celarier* [1997] at 1° × 1.25° resolution based on 14.5 years of TOMS measurements (360 nm). White locations on the map that indicate less than five suitable measurements were available in that season over the 3 year period. Differences in white space arise from resolution.

Table 2. Comparison of the NISE Classification in the OMI Snow Flag to Collocated Ground-Based Measurements of Snow Depth[a]

NISE Classification	Fraction of Observations With No Snow (0 cm)	Fraction of Observations With Thin Snow (0 < Snow Depth ≤ 5 cm)	Fraction of Observations With Thick Snow (Snow Depth > 5 cm)
Snow-free land 3872 observations	0.31	0.49	0.20
Dry snow 4301 observations	0.06	0.18	0.76

[a]For the snow-free and dry snow classifications, a breakdown is given of the fraction of measurements that fall into three different snow depth categories. The data are from November, December, January, February, and March of 2005 and 2006 over Edmonton and Calgary, Canada.

0.1 over the deserts of Saudi Arabia between March and August. GOME MinLER is higher for oceans by up to 0.04. Seasonal snow cover could contribute to the discrepancies at northern high latitudes where GOME MinLER is up to 0.1 higher.

4. Climatology of Snow-Covered Surface LER

[23] Here we develop a climatology of snow-covered surface LER and examine its dependence on season and vegetation before comparing with previous climatologies.

4.1. Data Set Development

[24] We first evaluate the usefulness of using the NISE data set to determine if an OMI scene is snow covered by comparing the snow flag to collocated ground-based measurements of snow depth. Snow-on-ground data are from the Canadian Daily Climate Data collected by Environment Canada (http://climate.weatheroffice.ec.gc.ca/) at the Calgary and Edmonton airports. These cities were chosen for the homogeneity of the surrounding land (no nearby large bodies of water) and occurrence of both snow-covered and snow-free scenes. The ground-based measurements are determined to be collocated with the OMI measurement if the OMI pixel center is within 0.5° (~50 km) of the airport. We divide snow depths into three categories: snow free, thin snow (up to 5 cm), and thick snow (more than 5 cm.) Data from the months of November, December, January, February, and March of 2005 and 2006 (10 months in total) are used in this comparison. This corresponds to a total of 8173 OMI pixels, 53% flagged as dry snow and 47% flagged as snow free. Snow cover data for April were unavailable for most airports.

[25] Table 2 shows the fraction of ground-based observations which fall into each of the three snow depth categories as a function of the NISE snow flag. Only 6% of the measurements with the NISE dry snow classification showed no snow on ground for that day at the nearby airport. However, for measurements with the snow-free classification, 69% had at least some snow on ground for that day at the nearby airport and 20% had snow depths of more than 5 cm. We conclude that the NISE dry snow classification is a good indication that a scene contains snow but that the snow-free classification is unreliable in regions that could contain seasonal snow cover. Spatial sampling bias is an unlikely explanation. Increasing the collocation criteria to 0.1° (~10 km) decreases to 5% (215 observations) the fraction of dry snow scenes with no snow on ground but increases to 74% (207 observations) the fraction of snow-free scenes with at least some snow on ground.

[26] We develop a data set of snow-covered surface reflectivity by using the mean surface LER viewed by OMI for scenes that are cloud free, as determined with the MODIS cloud mask, and snow covered, as flagged in the OMI product according to the NISE data set.

[27] Figure 3 (top) shows the mean observed LER of seasonal snow covered lands at 354 nm. The resulting LER depends strongly on the local vegetation type. The transition from the northern Canadian boreal forest (LER ~ 0.4) through the taiga to the arctic tundra (LER ~ 0.9) demonstrates the role of tall vegetation in masking the highly reflective snow [*Moody et al.*, 2007]. The prairies of central North America and Asia are highly reflective (LER ~ 0.8). Mountainous regions, such as the Tibetan Plateau, exhibit non-Lambertian behavior and have low LERs (~0.1) even when snow is present. Low LER values in the southeastern United States may arise from transient snow and a temporal mismatch of a few days between the SSM/I and OMI observations.

[28] Strict cloud screening leads to the rejection of nearly all OMI data over many locations in winter months. To increase the spatial extent of our data set, we relax the cloud screening algorithm. Our cloud-filtered data set is extended by only designating grid cells as contaminated if they contain clouds with optical depths greater than one. We account for the horizontal displacement of these optically thick clouds as before.

[29] Figure 3 (bottom) shows the mean surface LERs calculated using this relaxed cloud screening criteria. The LERs from this expanded data set are similar to those from the strictly cloudless data though the spatial coverage is improved. Forested regions have mean LERs as low as 0.3 even in the presence of snow. We examined the effect of relaxing the cloud screening criteria by comparing the newly accepted LER measurements to those that are part of the strictly cloud-free data set. The two data sets typically agree to within 0.05. Exceptions are over the bright prairies where clouds reduce the LER by approximately 0.1 and over the Tibetan Plateau where clouds increase the surface LER by approximately 0.15.

[30] We examine the temporal variability in the snow-covered LER to estimate the potential of using the expanded data set as a reliable measure of the snow-covered surface reflectivity. Standard deviations of the LERs throughout Canada and Russia are typically less than 0.15. These low standard deviations indicate that the surface reflectivity of snow-covered surfaces is represented within 10%–20%. Higher standard deviations of up to 0.3 to the south indicate

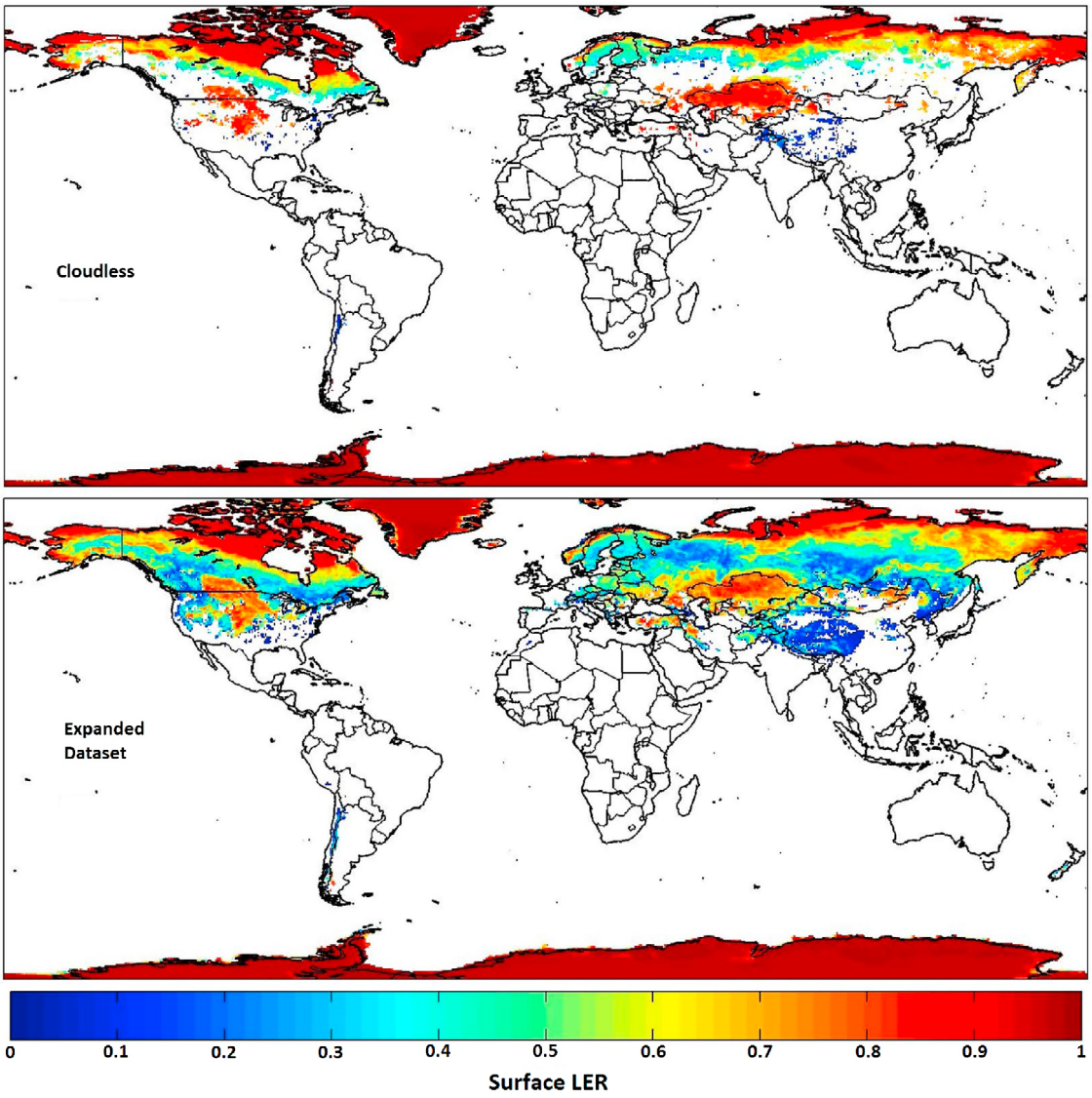

Figure 3. Annual mean surface LER of snow-covered scenes at 354 nm. (top) Strictly cloud free. (bottom) Relaxed cloud screening criteria (only scenes with cloud optical depths greater than 1 are rejected).

that snow-covered surface reflectivity is difficult to predict in regions with thin or transient snow.

4.2. Sensitivity to Vegetation

[31] Here we examine the dependence of our expanded snow-covered surface LER data set on the underlying vegetation type. We use the MODIS land cover product (MOD12C1) to determine the percentage of each International Geosphere-Biosphere Programme (IGBP) land cover type in each grid cell. We mask mountainous regions due to their non-Lambertian behavior. We then estimate the reflectivity of the various snow-covered land types in two different ways. The first method uses only pixels containing at least 95% of a single vegetation type. The second uses the maximum land cover type of each grid cell. This corresponds to the land cover type that occupies the largest fraction of the grid cell.

[32] Table 3 shows the LER of the snow-covered land types calculated in these two different ways. The differences between the mean LERs using the two methods reflect both the low sampling over some land cover types and the complex interaction of the vegetation types in determining the overall optical properties of the surface. The large variation with vegetation type has been well documented [*Robinson and Kukla*, 1985; *Arola et al.*, 2003; *Tanskanen and Manninen*, 2007]. This is due to the tops of the vegetation that extend beyond the snow-covered surface, thus partially obscuring the highly reflective snow from the satellite instrument [*Moody et al.*, 2007].

[33] Table 3 also includes vegetation dependence from previous work. *Tanskanen and Manninen* [2007] provide snow-covered LER estimates for locations containing at least 95% of a single vegetation type. Our results are similar except for cropland, which corresponds to largely different regions in their land cover type database when compared to

Table 3. OMI-Derived Surface LER of Various Snow-Covered Land Types[a]

Vegetation Type	LER for 95% Vegetation 354 nm	LER for Max Vegetation 354 nm	LER for 95% Vegetation 360 nm [*Tanskanen and Manninen*, 2007]	LER for Max Vegetation 470 nm [*Moody et al.*, 2007]
Water (lakes)	0.82	0.82	…	…
Evergreen needle-leaf forest	0.22	0.38	0.28	0.36
Deciduous needle-leaf forest	0.32	0.39	0.30	0.43
Deciduous broadleaf forest	…	0.17	…	0.43
Mixed forest	0.21	0.32	…	0.39
Open shrubland	0.80	0.75	0.83	0.73
Woody savannas	…	0.50	…	0.47
Grasslands	0.76	0.75	0.72	0.72
Permanent wetlands	…	0.70	…	0.69
Croplands	0.71	0.66	0.38	0.76
Cropland/natural vegetation mosaic	…	0.66	…	0.65

[a]The IGBP percentage land types are taken from the MODIS land cover product. The first method (95%) uses only grid squares containing at least 95% of a single land type to infer the mean LER. The second method (Max Vegetation) uses the maximum land cover type for each grid square. Results from two other sources are presented for comparison.

the MODIS land cover product. *Moody et al.* [2007] provide snow-covered albedo estimates for various maximum land types. Their results are consistent with ours with the exception of the albedo over deciduous broadleaf forests. This land cover type is the least sampled in our data set and may not be well represented.

4.3. Seasonal Variation

[34] The reflectivity of snow-covered lands further depends on several factors that change with time. We assess the seasonal variation of the snow-covered surface LERs using the monthly mean from grid cells that contain data for all 6 months, November through April.

[35] Figure 4 shows the observed mean seasonal variation in LER of snow-covered surfaces in the Northern Hemisphere. Reflectivity increases until January and then decreases through to April. The reflectivity of snow increases with solar zenith angle [*Wiscombe and Warren*, 1980]; however, *Arola et al.* [2003] argue that snow depth is the most crucial parameter in determining variation in the surface reflectivity. Deposition of soot and increase in grain size also lower the reflectivity of snow as it ages [*Warren and Wiscombe*, 1980]. During the melting season, the LER drops by 0.1, likely due to decreases in snow depth. Temporal mismatch between OMI and SSM/I may further contribute to the decrease in reflectivity.

4.4. Comparison With Existing Climatologies

[36] Figure 5 shows the difference between our snow-covered surface reflectivity database versus the three previous climatologies in winter months. GOME and TOMS MinLER are, by design, measures of the surface LER under conditions of minimal snow cover. This leads to both climatologies being lower than our snow-covered surface reflectivities. The OMI LER product allows for more than minimal snow cover in their surface reflectivities leading to LERs that are more consistent with our snow-covered surface LERs. However, regions such as the plains of south central Canada remain with large differences because of irregular but highly reflective snow cover. Locations where our snow-covered surface LER data set is lower than the OMI LER product, such as the Pacific coast of Canada and Eastern Europe, could indicate cloud contamination in the OMI LER product in winter months, since the surface reflectivity is expected to be at a maximum when snow is present.

[37] The large differences between our snow-covered product and all three previous climatologies demonstrate the difficulty in using a single value for the surface LER, in regions where seasonal snow cover is potentially present. It is therefore desirable to have two separate LERs in retrievals of atmospheric constituents: one for the snow-free case and one for the snow-covered case.

5. UV-Vis Trace Gas Retrievals Over Snow

[38] Trace gas retrievals using solar backscatter over regions of seasonal snow often are considered unreliable due to the difficulty in detecting snow, the uncertainty in its reflectivity, and the difficulty in detecting clouds in the

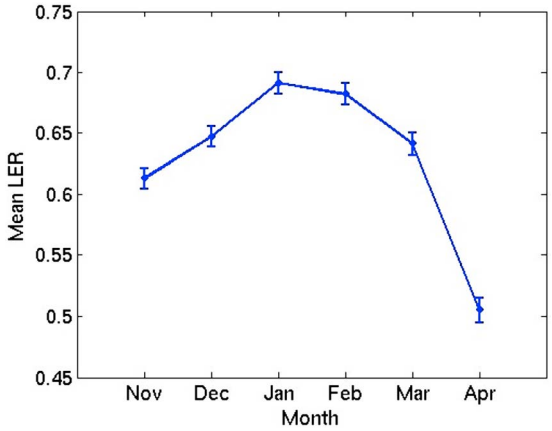

Figure 4. Monthly mean LER of seasonal snow-covered lands at 354 nm in the Northern Hemisphere. Only locations with clear-sky observations of nonclimatological snow cover for all 6 months (November–April) are used in computing the mean LER. Mountainous regions are masked. Error bars represent the standard deviation of the spatial mean.

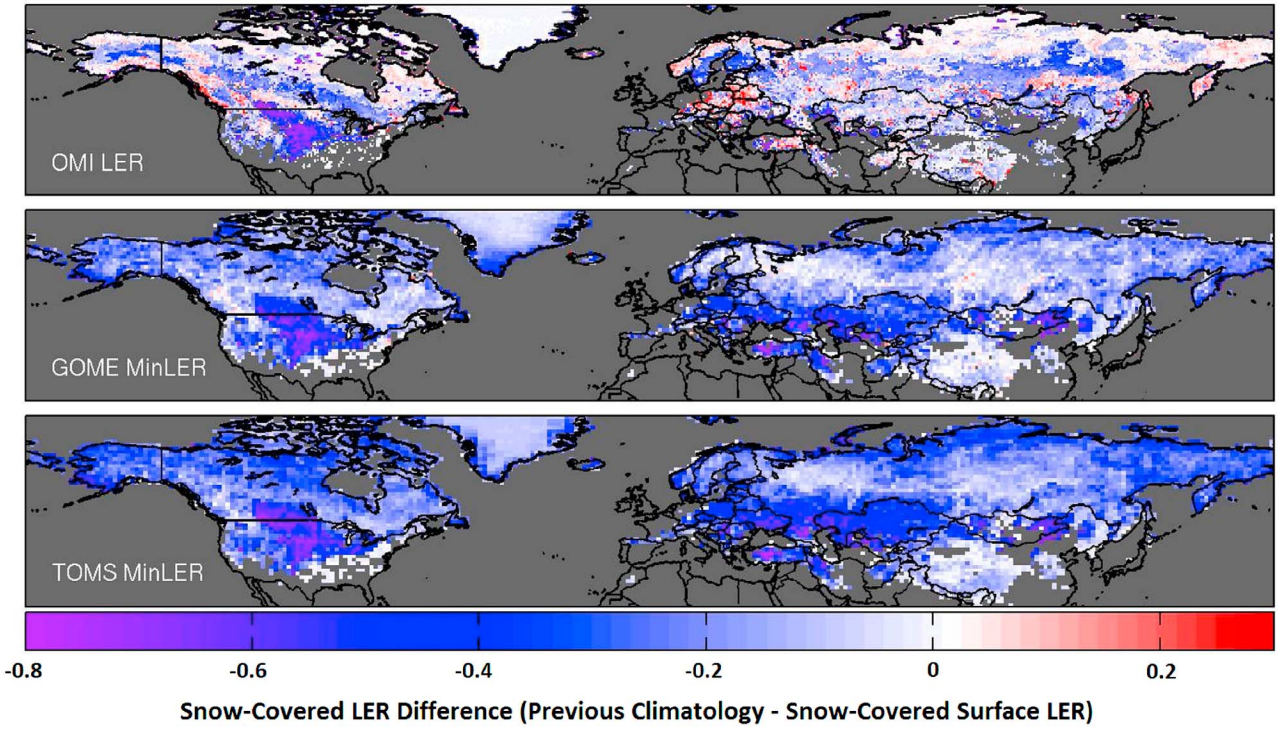

Figure 5. Difference between three previous surface LER climatologies and our snow-covered surface LERs for months where snow is observed by OMI: (top) surface LER from OMI (354 nm) [*Kleipool et al.*, 2008], (middle) surface reflectivity from GOME (interpolated 354 nm) [*Koelemeijer et al.*, 2003], and (bottom) surface reflectivity from TOMS (360 nm) [*Herman and Celarier*, 1997].

presence of snow. Should these difficulties be overcome, a snow-covered scene provides a better trace gas measurement than a snow-free scene. We explore the effect of snow on UV-Vis trace gas retrievals using tropospheric NO_2 as an example.

[39] Our snow-covered surface LER database is measured at 354 nm, whereas the OMI NO_2 retrieval is centered on 435 nm. However, the wavelength difference is of little consequence for our analysis due to the weak spectral dependence of snow in the UV-Vis. *Feister and Grewe* [1995] report that the albedo of a thin snow layer (2 cm) on grass rises from 0.656 at 350 nm to 0.678 at 440 nm. In the data set compiled by *Kleipool et al.* [2008], we find a mean difference of 0.006 between the surface reflectivities at 354 and 440 nm in regions where snow is observed.

[40] Figure 6 shows the effect of surface reflectivity on the random error in the AMF for tropospheric NO_2. Tropospheric AMFs are calculated for each surface reflectivity using a modeled NO_2 profile over the city of Edmonton, Canada. The tropospheric column errors are then generated using the formulation of *Wenig et al.* [2008]. Error in the tropospheric AMF is often the dominant term in polluted regions. Figure 6 indicates that for cloud-free scenes over cities the random error in the tropospheric AMF decreases from 25% over a nonreflective surface to 3% over a surface with a reflectivity of 0.4. This improvement is due to the increased sensitivity to the lower atmosphere, where the majority of the NO_2 column is located.

[41] Figure 7 shows the OMI tropospheric NO_2 column (including NO_2 below cloud) from the standard product [*Bucsela et al.*, 2006] over the cities of Calgary and Edmonton for the three different snow-on-ground categories described in section 4.1. OMI NO_2 columns over thick snow are 60% larger than those over snow-free surfaces. NO_2 columns in conditions reported as completely cloudy are a factor of four larger than those for cloud-free conditions. We compare to hourly in situ measurements taken at various locations in the two cities as part of the National Air Pollution Surveillance (NAPS) network. In contrast, these ground-based measurements exhibit only 13% higher NO_2

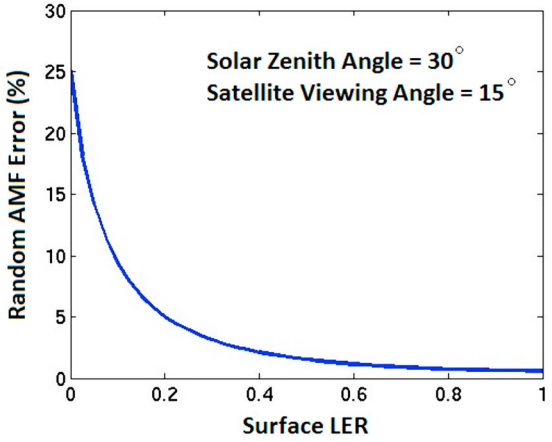

Figure 6. Random AMF error versus surface reflectivity for tropospheric NO_2 over Edmonton, Canada.

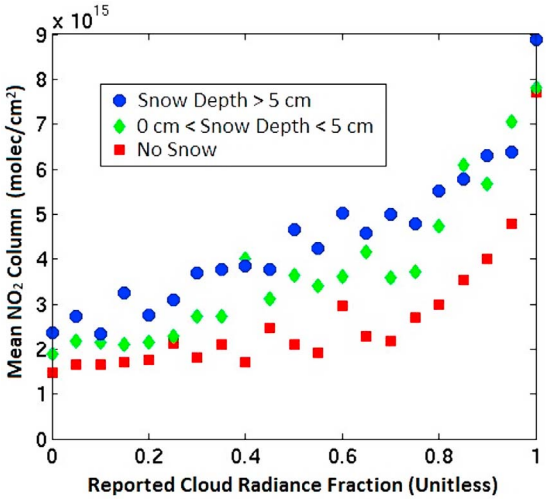

Figure 7. Mean OMI tropospheric NO_2 columns as a function of OMI-reported cloud radiance fraction for varying degrees of snow cover. The cloud radiance fraction is from the OMI NO_2 product based on the cloud fraction from the OMICLDO2 product. Red squares, no snow; green diamonds, snow-on-ground depth between 0 and 5 cm; blue circles, snow-on-ground depth of 5 cm or greater. Ten months of data (January, February, March, November, and December from 2005 and 2006) over two Canadian cities (Calgary and Alberta) are presented. The tropospheric NO_2 columns are binned according to reported cloud fraction and averaged. Snow depth is determined from ground-based measurements at local airports.

concentrations over thick snow compared to snow free and have no trend (r = 0.15) with reported cloud fraction. The bias arises from both false cloud detection and underestimates in surface reflectivity as discussed below. Errors in the a priori surface reflectivity will introduce errors in the OMI cloud fraction retrieval, so we make the distinction between the cloud fractions reported in the OMI product and real cloud fractions.

[42] The surface LER affects the AMF calculation both directly and through the cloud retrieval. Both of these aspects need to be considered when correcting the NO_2 retrieval over snow for errors in the a priori surface LER. We address the direct effect by using our climatology of snow-covered surface LERs and the cloud effect by only using scenes from our expanded cloud-free data set. For each of these cloud-free scenes, two AMFs are calculated at 440 nm. The first is calculated with the original surface LER and reported cloud fraction. The second (corrected) AMF is calculated using our snow-covered surface LER and a cloud fraction of zero. Relative differences in these two AMFs are used to infer relative biases in the tropospheric NO_2 column for scenes flagged as snow covered. Both OMI NO_2 retrievals (standard and DOMINO) currently use the same cloud and surface LER data so our results are applicable to both products.

[43] Figure 8 (top) shows the mean relative bias in the OMI NO_2 retrieval over snow. Retrievals over highly reflective snow-covered grasslands overestimate the tropospheric NO_2 column by more than 100%. These regions exhibit large underestimates of the surface reflectivity for snow-covered scenes (Figure 5), which leads to underestimates in the sensitivity to NO_2 in the lower atmosphere. This, in turn, leads to overestimates in the total NO_2 column. Elsewhere, blue regions in Figure 8 (top) reveal underestimates in the NO_2 columns over snow that arise from overestimates in the surface LER. Snow-related bias in the NO_2 retrieval is smaller in the northernmost regions where snow cover is better represented.

[44] Though only cloud-free scenes (as inferred from MODIS) are used in this analysis, nonzero cloud fractions are commonly reported in the OMICLDO2 product due to

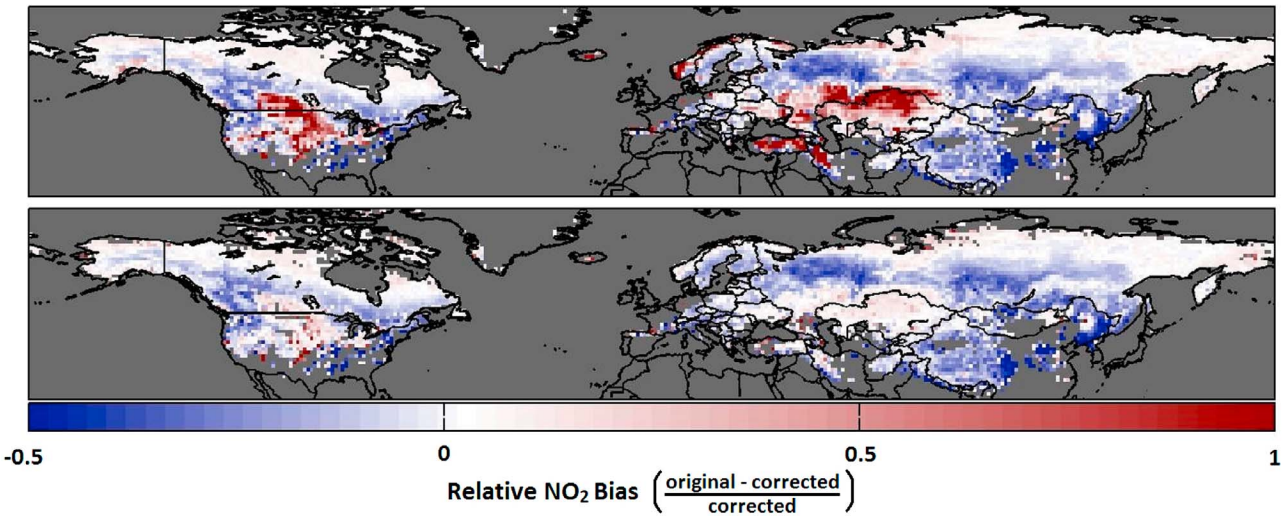

Figure 8. (top) Calculated relative bias in the tropospheric NO_2 retrieval from OMI for cloud-free (determined by MODIS) and snow-covered (determined by the NISE data set) scenes. Two years of data (2005 and 2006) are used to calculate the relative bias. (bottom) Same as top, but scenes with OMI-reported cloud fraction greater than 0.3 are rejected.

errors in the a priori surface LER. In snow-covered regions, the lack of contrast between cloud and surface exacerbates this problem. We find that any cloud fraction can be reported in OMICLDO2, even for MODIS-determined cloud-free scenes. In a typical study of mean NO_2 columns, scenes with cloud fractions greater than a certain threshold (for example, 0.3 or 0.5) are rejected to ensure sensitivity to the surface in all measurements.

[45] Figure 8 (bottom) shows the mean bias in the OMI tropospheric NO_2 retrieval for (MODIS determined) cloud-free scenes when an OMI cloud fraction threshold of 0.3 is applied. The overestimates evident in Figure 8 (top) are reduced to less than 20%. This is because an underestimate of the surface reflectivity yields an overestimate in the cloud fraction, which increases the likelihood that the scene will be rejected as cloudy. The low biased regions in Figure 8 (top) are, however, largely unaltered because an overestimate in surface reflectivity will ensure a cloud fraction of zero is reported. Though this study is confined to cloud-free scenes, the trend of underestimating NO_2 in regions where the surface reflectivity is overestimated and rejecting scenes where the surface reflectivity is underestimated will persist for most partially cloudy scenes. This implies that mean NO_2 columns tend to be underestimated over snow-covered surfaces where the surface LER is poorly characterized. Future cloud and trace gas retrievals would benefit from a separate surface LER database for snow-covered scenes. The general effects found here for NO_2 should be similar for other trace gas retrievals in the UV-Vis.

6. Conclusion

[46] We have created a database of surface reflectivity at 354 nm using observations from two satellite instruments in the A-Train. MODIS/Aqua observations were used to identify and exclude scenes contaminated by cloud and aerosol. OMI observations of the resultant clear-sky scenes were used to determine the Lambertian equivalent reflectivity (LER) of both snow-free and snow-covered lands. We applied this database to evaluate previous surface LER climatologies from TOMS, GOME, and OMI. Our snow-free cloud- and aerosol-filtered surface LERs, where available, agree well (mean difference, 0.0002; standard deviation, 0.011) with the OMI LER [*Kleipool et al.*, 2008] climatology. Differences of up to 0.05 remain over regions with a large dust influence. Other climatologies which select the minimum observed LER as the surface LER, exhibit greater discrepancies (mean difference >0.002; standard deviation >0.02) versus our cloud- and aerosol-filtered data set.

[47] Our analysis focused on LER, as currently used in OMI retrievals. In reality, the surface reflectivity has angular dependence. An improved description of the surface reflectivity, which better characterizes the bidirectional reflectance function, should improve future retrievals using solar backscatter.

[48] We evaluated surface LER characteristics for snow-covered lands at 354 nm. Our snow-covered surface reflectivity database depends strongly on the underlying vegetation. Surface LERs range from 0.3 for some forested regions to 0.8 over shrubland. The mean LER of snow-covered lands in the Northern Hemisphere increases by 0.1 from November to January and decreases by 0.1 through March. None of the previous climatologies used in trace gas retrievals agree well with our mean snow-covered surface LERs in winter months. This is largely by design as TOMS MinLER and GOME MinLER report the surface LERs for minimum snow cover. OMI LER allows for a contribution to the surface LER by snow, but this leads to some cloud contamination in winter months. Furthermore, including seasonal snow in the climatological surface LER leads to ambiguity in surface LER and therefore in trace gas retrievals over snow. We propose the use of a separate surface LER database for snow-covered scenes.

[49] We investigated the effect of seasonal snow cover on UV-Vis trace gas retrievals using NO_2 as an example. The weak spectral dependence of snow in the UV-Vis allows application of our data set at 354 nm for OMI NO_2 retrievals at 440 nm. OMI NO_2 retrievals over central Canada exhibit dependence on cloud and snow that is inconsistent with in situ measurements. Underestimates in the snow-covered surface reflectivity lead to overestimates in the OMI NO_2 and cloud fraction retrievals, even when no clouds are present in the field of view of the instrument. These scenes tend to get rejected by cloud fraction filters due to the overestimated cloud fractions. Conversely, overestimates of the surface reflectivity lead to underestimates in both the OMI NO_2 and cloud fraction retrievals. These scenes are then preferentially accepted by cloud fraction filters because of the artificially low cloud fractions. The net effect is that NO_2 columns tend to be underestimated over seasonal snow-covered lands if a cloud fraction filter is applied. Random errors in the surface reflectivity will also lead to systematic underestimates in the NO_2 column when a cloud fraction filter is used. This is because scenes where the surface reflectivity is underestimated tend to underestimate NO_2 and are preferentially selected by the cloud fraction filter.

[50] If well characterized, snow increases the sensitivity of UV-Vis retrievals to trace gases in the lower troposphere. However, snow detection is challenging, and we find that the NISE snow-free classification is less reliable for OMI scenes in regions containing thin snow cover. OMI products could benefit from the use of a validated data set such as the MODIS snow cover product [*Hall and Riggs*, 2007]. Emerging snow/ice/cloud data from SCIAMACHY [*Krijger et al.*, 2005; *Lotz et al.*, 2009] may be useful for future work. We did not explore the effects of scenes that are incorrectly flagged (either as snow covered or snow free) on the retrieved mean NO_2 columns. In addition, partially cloudy scenes could be affected to a different degree than the clear-sky scenes used in our comparisons. For these reasons, our results should only be used as guidelines for assessing the effect of snow on the OMI NO_2 retrieval and not as a quantitative measure of the overall bias due to snow. Future satellite missions to measure trace gases using solar backscatter would benefit from additional discrete spectral bands at longer wavelengths to improve discrimination between cloud and snow.

[51] **Acknowledgments.** Terry O'Byrne and two anonymous reviewers provided helpful comments that improved this manuscript. We thank the OMI and MODIS teams as well as Environment Canada for making their data publicly available. This research was supported by NASA and the Canadian Foundation for Climate and Atmospheric Science.

References

Acarreta, J. R., J. F. De Haan, and P. Stammes (2004), Cloud pressure retrieval using the O2-O2 absorption band at 477 nm, *J. Geophys. Res.*, *109*, D05204, doi:10.1029/2003JD003915.

Ackerman, S. A., K. I. Strabala, W. P. Menzel, R. A. Frey, C. C. Moeller, and L. E. Gumley (1998), Discriminating clear sky from clouds with MODIS, *J. Geophys. Res.103*(D24)32,141–32,157, doi:10.1029/1998JD200032.

Ackerman, S. A., R. E. Holz, R. Frey, E. W. Eloranta, B. C. Maddux, and M. McGill (2008), Cloud detection with MODIS: part II. Validation, *J. Atmos. Oceanic Technol.*, *25*, 1073–1086, doi:10.1175/2007JTECHA1053.1.

Armstrong, R. L., and M. J. Brodzik (2001), Recent Northern Hemisphere snow extent: A comparison of data derived from visible and microwave satellite sensors, *Geophys. Res. Lett.*, *28*(19), 3673–3676, doi:10.1029/2000GL012556.

Armstrong, R. L., and M. J. Brodzik (2002), Hemispheric-scale comparison and evaluation of passive-microwave snow algorithms, *Ann. Glaciology*, *34*, 38–44.

Arola, A., J. Kaurola, L. Koskinen, A. Tanskanen, T. Tikkanen, P. Taalas, J. R. Herman, N. Krotkov, and V. Fioletov (2003), A new approach to estimating the albedo for snow-covered surfaces in the satellite UV method, *J. Geophys. Res.*, *108*(D17), 4531, doi:10.1029/2003JD003492.

Beirle, S., U. Platt, M. Wenig, and T. Wagner (2003), Weekly cycle of NO2 by GOME measurements: A signature of anthropogenic sources, *Atmos. Chem. Phys.*, *3*, 2225–2232.

Berendes, T. A., D. A. Berendes, R. M. Welch, E. G. Dutton, T. Uttal, and E. E. Clothiaux (2004), Cloud cover comparisons of the MODIS daytime cloud mask with surface instruments at the North Slope of Alaska ARM site, *IEEE Trans. Geosci. Remote Sens.*, *42*, 2584–2593, doi:10.1109/TGRS.2004.835226.

Boersma, K. F., H. J. Eskes, and E. J. Brinksma (2004), Error analysis for tropospheric NO_2 retrieval from space, *J. Geophys. Res.*, *109*, D04311, doi:10.1029/2003JD003962.

Boersma, K. F., et al. (2007), Near-real time retrieval of tropospheric NO_2 from OMI, *Atmos. Phys., Chem.*, *7*, 2103–2118.

Boersma, K. F., D. J. Jacob, H. J. Eskes, R. W. Pinder, J. Wang, and R. J. van der A (2008), Intercomparison of SCIAMACHY and OMI tropospheric NO_2 columns: Observing the diurnal evolution of chemistry and emissions from space, *J. Geophys. Res.*, *113*, D16S26, doi:10.1029/2007JD008816.

Bucsela, E. J., E. A. Celarier, M. O. Wenig, J. F. Gleason, J. P. Veefkind, K. F. Boersma, and E. J. Brinksma (2006), Algorithm for NO_2 vertical column retrieval from the ozone monitoring instrument, *IEEE Trans. Geosci. Remote Sens.*, *44*, 1245–1258, doi:10.1109/TGRS.2005.863715.

Chance, K. (1998), Analysis of BrO measurements from the Global Ozone Monitoring Experiment, *Geophys. Res. Lett.*, *25*(17), 3335–3338, doi:10.1029/98GL52359.

Chance, K. (2006), Spectroscopic measurements of tropospheric composition from satellite measurements in the ultraviolet and visible: Steps toward continuous pollution monitoring from space, in *Remote Sensing of the Atmosphere for Environmental Security*, edited by A. Perring, N. Ben Sari-Zizi, and J. Demaison, pp. 1–25, Springer, New York.

Chang, A. T. C., J. L. Foster, and D. K. Hall (2002), Nimbus-7 SMMR derived global snow cover paramters, *Ann. Glaciol.*, *9*, 39–44.

Davé, J. V. (1964), The meaning of successive iteration of the auxiliary equation in the theory of radiative transfer, *Astrophys. J.*, *140*, 1292.

Feister, U., and R. Grewe (1995), Spectral albedo measurements in the UV and visible region over different types of surfaces, *Photochem. Photobiol.*, *62*(4), 736–744.

Fishman, J., K. Fakhruzzaman, B. Cros, and D. Nganga (1991), Identification of widespread pollution in the Southern Hemisphere deduced from satellite analyses, *Science*, *252*(5013), 1693–1696.

Fishman, J., et al. (2008), Remote sensing of tropospheric pollution from space, *Bull. Am. Meteorol. Soc.*, *89*, 805–821, doi:10.1175/2008BAMS2526.1.

Hall, D. K., and G. A. Riggs (2007), Accuracy assessment of the MODIS snow products, *Hydrol. Processes*, *21*, 1534–1547, doi:10.1002/hyp.6715.

Herman, J. R., and E. A. Celarier (1997), Earth surface reflectivity climatology at 340–380 nm from TOMS data, *J. Geophys. Res.*, *102*(D23), 28,003–28,011, doi:10.1029/97JD02074.

Herman, J. R., P. K. Bhartia, O. Torres, C. Hsu, C. Seftor, and E. Celarier (1997), Global distribution of UV-absorbing aerosols from Nimbus 7/TOMS data, *J. Geophys. Res.102*(D14), 16,911–16,922, doi:10.1029/96JD03680.

Joiner, J., and A. P. Vasilkov (2006), First results from the OMI rotational Raman scattering cloud pressure algorithm, *IEEE Trans. Geosci. Remote Sens.*, *44*, 1272–1282, doi:10.1109/TGRS.2005.861385.

Kleipool, Q. L., M. R. Dobber, J. F. de Haan, and P. F. Levelt (2008), Earth surface reflectance climatology from 3 years of OMI data, *J. Geophys. Res.*, *113*, D18308, doi:10.1029/2008JD010290.

Koelemeijer, R. B. A., P. Stammes, J. W. Hovenier, and J. F. de Haan (2001), A fast method for retrieval of cloud parameters using oxygen A band measurements from the Global Ozone Monitoring Experiment, *J. Geophys. Res.*, *106*(D4), 3475–3490, doi:10.1029/2000JD900657.

Koelemeijer, R. B. A., J. F. de Haan, and P. Stammes (2003), A database of spectral surface reflectivity in the range 335–772 nm derived from 5.5 years of GOME observations, *J. Geophys. Res.*, *108*(D2), 4070, doi:10.1029/2002JD002429.

Krijger, J. M., I. Aben, and H. Schrijver (2005), Distinction between clouds and ice/snow covered surfaces in the indentification of cloud-free observations using SCIAMACHY PMDs, *Atmos. Chem. Phys.*, *5*, 2729–2738.

Krotkov, N. A., J. R. Herman, P. K. Bhartia, V. Fioletov, and Z. Ahmad (2001), Satellite estimation of spectral surface UV irradiance: 2. Effects of homogeneous clouds and snow, *J. Geophys. Res.*, *106*(D11), 11,743–11,759, doi:10.1029/2000JD900721.

Krueger, A. J. (1983), Sighting of El-Chichon sulfur-dioxide clouds with the Nimbus-7 total ozone mapping spectrometer, *Science*, *220*(4604), 1377–1379.

Lamsal, L. N., R. V. Martin, A. van Donkelaar, M. Steinbacher, E. A. Celarier, E. Bucsela, E. J. Dunlea, and J. P. Pinto (2008), Ground-level nitrogen dioxide concentrations inferred from the satellite-borne Ozone Monitoring Instrument, *J. Geophys. Res.*, *113*, D16308, doi:10.1029/2007JD009235.

Lee, C., R. V. Martin, A. van Donkelaar, G. O'Byrne, A. Richter, G. Huey, and J. S. Holloway (2009), Retrieval of vertical columns of sulfur dioxide from SCIAMACHY and OMI: Air mass factor algorithm development and validation, *J. Geophys. Res.*, *114*, D22303, doi:10.1029/2009JD012123.

Levelt, P. F., G. H. J. Van den Oord, M. R. Dobber, A. Malkki, H. Visser, J. de Vries, P. Stammes, J. O. V. Lundell, and H. Saari (2006), The Ozone Monitoring Instrument, *IEEE Trans. Geosci. Remote Sens.*, *44*, 1093–1101, doi:10.1109/TGRS.2006.872333.

Liu, Y. H., J. R. Key, R. A. Frey, S. A. Ackerman, and W. P. Menzel (2004), Nighttime polar cloud detection with MODIS, *Remote Sens. Environ.*, *92*, 181–194, doi:10.1016/j.rse.2004.06.004.

Lotz, W. A., M. Vountas, T. Dinter, and J. P. Burrows (2009), Cloud and surface classification using SCIAMACHY polarization measurement devices, *Atmos. Chem. Phys.*, *8*, 9855–9881.

Martin, R. V. (2008), Satellite remote sensing of surface air quality, *Atmos. Environ.*, *42*, 7823–7843, doi:10.1016/j.atmosenv.2008.07.018.

Martin, R. V., D. J. Jacob, K. Chance, T. P. Kurosu, P. I. Palmer, and M. J. Evans (2003), Global inventory of nitrogen oxide emissions constrained by space-based observations of NO_2 columns, *J. Geophys. Res.*, *108*(D17), 4537, doi:10.1029/2003JD003453.

Miller, R. L., et al. (2006), Mineral dust aerosols in the NASA Goddard Institute for Space Sciences ModelE atmospheric general circulation model, *J. Geophys. Res.*, *111*, D06208, doi:10.1029/2005JD005796.

Moody, E. G., M. D. King, C. B. Schaaf, D. K. Hall, and S. Platnick (2007), Northern Hemisphere five-year average (2000–2004) spectral albedos of surfaces in the presence of snow: Statistics computed from Terra MODIS land products, *Remote Sens. Environ.*, *111*, 337–345, doi:10.1016/j.rse.2007.03.026.

Müller, J. F., and T. Stavrakou (2005), Inversion of CO and NO_x emissions using the adjoint of the IMAGES model, *Atmos. Chem. Phys.*, *5*, 1157–1186.

Nolin, A., R. L. Armstrong, and J. Maslanik (1998), Near-Real-Time SSM/I EASE-Grid Daily Global Ice Concentration and Snow Extent (2004–present), digital media, Natl. Snow and Ice Data Cent., Boulder, Colo.

Palmer, P. I., D. J. Jacob, K. Chance, R. V. Martin, R. J. D. Spurr, T. P. Kurosu, I. Bey, R. Yantosca, A. Fiore, and Q. B. Li (2001), Air mass factor formulation for spectroscopic measurements from satellites: Application to formaldehyde retrievals from the Global Ozone Monitoring experiment, *J. Geophys. Res.*, *106*(D13), 14,539–14,550, doi:10.1029/2000JD900772.

Palmer, P. I., D. J. Jacob, A. M. Fiore, R. V. Martin, K. Chance, and T. P. Kurosu (2003), Mapping isoprene emissions over North America using formaldehyde column observations from space, *J. Geophys. Res.*, *108*(D6), 4180, doi:10.1029/2002JD002153.

Platnick, S., M. D. King, S. A. Ackerman, W. P. Menzel, B. A. Baum, J. C. Riedi, and R. A. Frey (2003), The MODIS cloud products: Algorithms and examples from Terra, *IEEE Trans. Geosci. Remote Sens.*, *41*(2), 459–473, doi:10.1109/TGRS.2002.808301.

Remer, L. A., et al. (2005), The MODIS aerosol algorithm, products, and validation, *J. Atmos. Sci.*, *62*, 947–973.

Richter, A., and J. P. Burrows (2002), Tropospheric NO_2 from GOME measurements, *Adv. Space Res.*, *29*(11), 1673–1683.

Richter, A., J. P. Burrows, H. Nuss, C. Granier, and U. Niemeier (2005), Increase in tropospheric nitrogen dioxide over China observed from space, *Nature*, *437*, 129–132, doi:10.1038/nature04092.

Robinson, D. A., and G. Kukla (1985), Maximum surface albedo of seasonally snow-covered lands in the Northern Hemisphere, *J. Clim. Appl. Meteorol.*, *24*(5), 402–411.

Salomonson, V. V., W. L. Barnes, P. W. Maymon, H. E. Montgomery, and H. Ostrow (1989), MODIS—Advanced facility instrument for studies of the Earth as a system, *IEEE Trans. Geosci. Remote Sens.*, *27*(2), 145–153.

Sneep, M., J. F. de Haan, P. Stammes, P. Wang, C. Vanbauce, J. Joiner, A. P. Vasilkov, and P. F. Levelt (2008), Three-way comparison between OMI and PARASOL cloud pressure products, *J. Geophys. Res.*, *113*, D15S23, doi:10.1029/2007JD008694.

Stammes, P., M. Sneep, J. F. De Haan, J. P. Veefkind, P. Wang, and P. F. Levelt (2008), Effective cloud fractions from the Ozone Monitoring Instrument: Theoretical framework and validation, *J. Geophys. Res.*, *113*, D16S38, doi:10.1029/2007JD008820.

Stutz, J., and U. Platt (1996), Numerical analysis and estimation of the statistical error of differential optical absorption spectroscopy measurements with least squares methods, *Appl. Opt.*, *35*(30), 6041–6053.

Tanskanen, A., and T. Manninen (2007), Effective UV surface albedo of seasonally snow-covered lands, *Atmos. Chem. Phys.*, *7*, 2759–2764.

Torres, O., P. K. Bhartia, J. R. Herman, Z. Ahmad, and J. Gleason (1998), Derivation of aerosol properties from satellite measurements of backscattered ultraviolet radiation: Theoretical basis, *J. Geophys. Res.*, *103*(D14), 17,099–17,110, doi:10.1029/98JD00900.

Wagner, T., S. Beirle, T. Deutschmann, E. Eigemeier, C. Frankenberg, M. Grzegorski, C. Liu, T. Marbach, U. Platt, and M. P. de Vries (2008), Monitoring of atmospheric trace gases, clouds, aerosols and surface properties from UV/vis/NIR satellite instruments, *J. Opt. A Pure Appl. Opt.*, *10*, 104019, doi:10.1088/1464-4258/10/10/104019.

Warren, S. G., and W. J. Wiscombe (1980), A model for the spectral albedo of snow: 2. Snow containing atmospheric aerosols, *J. Atmos. Sci.*, *37*(12), 2734–2745.

Wenig, M. O., A. M. Cede, E. J. Bucsela, E. A. Celarier, K. F. Boersma, J. P. Veefkind, E. J. Brinksma, J. F. Gleason, and J. R. Herman (2008), Validation of OMI tropospheric NO_2 column densities using direct-Sun mode Brewer measurements at NASA Goddard Space Flight Center, *J. Geophys. Res.*, *113*, D16S45, doi:10.1029/2007JD008988.

Wiscombe, W. J., and S. G. Warren (1980), A model for the spectral albedo of snow: 1. Pure snow, *J. Atmos. Sci.*, *37*(12), 2712–2733.

E. A. Celarier, Goddard Earth Sciences and Technology Center, University of Maryland Baltimore County, Baltimore, MD 21228, USA.

J. Joiner, NASA Goddard Space Flight Center, Greenbelt, MD 20771, USA.

R. V. Martin, G. O'Byrne, and A. van Donkelaar, Department of Physics and Atmospheric Science, Dalhousie University, Halifax, NS B3H 3J5, Canada. (randall.martin@dal.ca)